IOP Publishing Plasma Sources Science and Technology

Plasma Sources Sci. Technol. **24** (2015) 035006 (12pp) doi:10.1088/0963-0252/24/3/035006

A collisionless plasma thruster plume expansion model

Mario Merino, Filippo Cichocki and Eduardo Ahedo

Equipo de Propulsión Espacial y Plasmas (EP2), Universidad Carlos III de Madrid, Leganés, Spain

E-mail: mario.merino@uc3m.es

Received 20 November 2014, revised 18 February 2015
Accepted for publication 27 March 2015
Published 30 April 2015

Abstract

A two-fluid model of the unmagnetized, collisionless far region expansion of the plasma plume for gridded ion thrusters and Hall effect thrusters is presented. The model is integrated into two semi-analytical solutions valid in the hypersonic case. These solutions are discussed and compared against the results from the (exact) method of characteristics; the relative errors in density and velocity increase slowly axially and radially and are of the order of 10^{-2}–10^{-3} in the cases studied. The plasma density, ion flux and ambipolar electric field are investigated. A sensitivity analysis of the problem parameters and initial conditions is carried out in order to characterize the far plume divergence angle in the range of interest for space electric propulsion. A qualitative discussion of the physics of the secondary plasma plume is also provided.

Keywords: plasma plumes, self-similar models, cold plasma, plasma expansion, fluid models

(Some figures may appear in colour only in the online journal)

1. Introduction

The expansion of a plasma plume into vacuum is a recurring phenomenon in plasma space propulsion [1, 2], as well as other areas such as plasma material processing and astrophysics. Understanding and characterizing the distribution of the plasma density, temperatures, fluxes and electric potential in the plume that forms outside a plasma thruster, such as a gridded ion thruster (GIT) or Hall effect thruster (HET), is essential for determining the performance of the device and assessing its interaction with the rest of the spacecraft (electric charging, mechanical erosion and contamination [3, 4]) or any nearby object.

For satellite integrators there is naturally concern about the negative effect that the impingement of energetic ions can have on sensitive surfaces of a spacecraft when the plume divergence is large and due to stray high-energy particles. A greater divergence means also thrust efficiency losses, as a non-negligible fraction of the applied power is invested in accelerating the plasma radially instead of axially. Plume divergence is especially relevant in new, advanced uses of plasma propulsion such as in relation to the ion beam shepherd (IBS) concept, where a plasma beam is directed against a target orbiting object (space debris, asteroids, etc) in order to contactlessly reposition it [5–7].

The propulsive plasma plume can be roughly divided into two distinct regions, as illustrated in figure 1. Firstly, close to the thruster, the plasma can be markedly non-homogeneous. For instance, a GIT exhaust consists of numerous 'beamlets' that gradually merge into a single beam and a HET plume has a profile that is initially annular. The thruster and external neutralizer mix their fluxes and 3D effects dominate due to the asymmetry introduced by the latter. The applied electric and magnetic fields of the thruster may affect the expansion: e.g. in a GIT there is a potential well at the last grid and in a HET the magnetic field extends some distance outside of the thruster. Lastly, the presence of neutrals in this region indicates a stronger influence of momentum-exchange and charge-exchange collisions. This is the complex *near region*, which extends for about 1–2 thruster radii for GITs [8, 9] and HETs [10, 11] downstream from the thruster exit. Afterwards, a smooth, single-peaked plasma profile forms and these effects become negligible with respect to the plume kinetic energy, the residual thermal pressure and the self-consistent ambipolar electric field that develops in the plasma. The subsequent plasma expansion is essentially current-free, quasineutral and

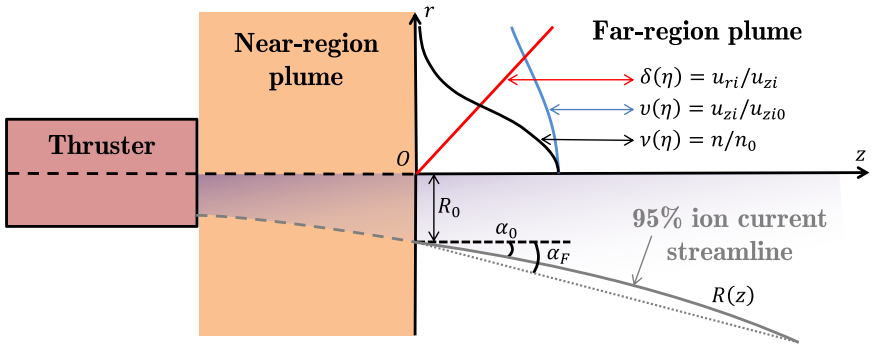

Figure 1. Sketch of a plasma plume's near and far regions and the plasma streamtube $R(z)$ containing 95% of the ion current. The reference plane that serves as the initial condition for the far region, typical shapes for the initial profiles of the velocity slope, axial velocity and density (δ, υ, ν), the initial divergence angle, α_0 and the equivalent far-region divergence angle, α_F, are shown schematically.

nearly collisionless. Typically, the initial divergence angle of the beam, defined as the half-angle of the plasma tube that contains 95% of the ion flux at the beginning of the far region, is roughly 10°–20° for GITs and 40°–50° for HETs [12]. The divergence angle of this plasma tube continues to increase downstream as dictated by its thermal pressure and the ambipolar electric field.

In this *far region*, the plume is constituted of highly hypersonic ions with velocity u_i of the order of tens of kilometers per second and electrons with a mild temperature T_e of 0.1–5 eV [11, 13, 14] that are nearly confined by the electric field, with a drift velocity several orders of magnitude lower than their thermal velocity. The plasma densities decay from about 10^{16}–10^{18} m^{-3} to 10^{12}–10^{14} m^{-3} in a few meters [13].

The plume near region is investigated in laboratory experiments, where the plasma properties are routinely measured at distances of about 1 m from the exit of the thruster [9–11, 13, 15–17]. The far region (like the peripheral plasma), in contrast, presents serious challenges for vacuum chamber testing, as large vacuum tanks and high vacuum levels are required to limit the influence of the tank walls and the background plasma density on the measurements of the low-density plume and produce reliable data [1]. On the other hand, modeling and simulating the near region accurately is a difficult task due to the abundance of competing physical effects requiring complex numerical codes. Examples of existing simulation techniques include the use of advanced particle-in-cell (PIC) codes and hybrid PIC–fluid codes [4, 18, 19]. In contrast, the far region is amenable to investigation using simpler models such as collisionless fluid models. These models confer a clearer understanding of the main physics of the problem and can be used to propagate experimental data downstream, extrapolate vacuum chamber measurements to space conditions and identify effects of facilities on far region measurements. This paper presents a two-fluid model of the nearly collisionless expansion of the far region into the vacuum of unmagnetized plasma plumes. Two semi-analytical methods are proposed that yield a deep insight into the physics of the expansion and a rapid solution, known as the *asymptotic expansion method* (AEM) and the *self-similar method* (SSM) [20, 21]. The latter generalizes the particular self-similar solutions proposed by Parks and Katz [22], Korsun and Tverdokhlebova [23] and Ashkenazy and Fruchtman [24]. The findings from the two semi-analytical methods are compared against the accurate solution from the method of characteristics (MoC). Lastly, the paper investigates the dominant plume physics, with special focus on the ambipolar electric field and the plume divergence angle and discusses qualitatively other physical effects that can play a role in the far region expansion.

The rest of the paper is structured as follows. Section 2 introduces the two-fluid model of the plasma plume far region. Sections 3 and 4 derive and discuss the two semi-analytical methods: AEM and SSM. The discussion of the plume physics is given in section 5. Finally, conclusions are summarized in section 6.

2. The far region plasma plume model

The far region plasma plume is nearly collisionless and unmagnetized and the dominant effects are the ion inertia, the electron pressure and the ambipolar electric field that relates the two charged species. The plasma profile has become smooth, meaning that in the bulk of the far region expansion the gradient length is of the order of the thruster radii (typically ~10 cm) or more, much greater than the Debye length (~1 mm or less), which means that the expansion can be considered quasineutral in most of the plume. We consider below the expansion of an axisymmetric, non-rotating plume from an initial reference plane $z = 0$, already in the far region. This reference plane can be chosen at e.g. 0.5–1 m, where the ion current and plasma density are typically measured in laboratory experiments.

With these considerations, the steady-state, far region plume expansion is macroscopically described by the following two-fluid equations for singly charged ions and non-rotating electrons:

$$n_i = n_e \equiv n, \tag{1}$$

$$\nabla \cdot (n\boldsymbol{u}_i) = 0, \tag{2}$$

$$\nabla \cdot (n\boldsymbol{u}_e) = 0, \tag{3}$$

$$nm_i(\boldsymbol{u}_i \cdot \nabla)\boldsymbol{u}_i = -en\,\nabla\phi, \tag{4}$$

$$0 = -\nabla \cdot \mathcal{P}_e + en\,\nabla\phi, \tag{5}$$

$$u_{\theta i} = u_{\theta e} = 0, \tag{6}$$

where ϕ is the ambipolar electric potential, $\mathcal{P}_e$ is the electron pressure tensor and the rest of symbols are conventional. In these equations, the ion thermal pressure and the electron inertia have been neglected, assuming the typical scaling of a propulsive plasma plume in the whole region of interest:

$$m_e u_e^2, T_i \ll T_e \ll m_i u_i^2.$$

A state equation from kinetic theory is needed to close the fluid model and provide the components of $\mathcal{P}_e$. Solving for the plasma plume at a kinetic level is a challenging task, beyond the scope of this paper, primarily focused on the discussion of the dominant macroscopic behavior and the derivation of semi-analytical plume solution methods. Hence, in the following, $\mathcal{P}_e$ is approximated as a diagonal (isotropic) tensor, such that $\nabla \cdot \mathcal{P}_e = \nabla p_e$, where $p_e = n\, T_e$ is the scalar electron pressure. Furthermore, a polytropic law is assumed, i.e.

$$T_e \propto n^{\gamma-1}, \tag{7}$$

as a simplified electron cooling model. The effective cooling rate γ can be tuned to fit experimental measurements, with $\gamma = 1$ corresponding to the isothermal limit and $\gamma = 5/3$ to an adiabatic plasma. In a first approximation, the high conductivity of collisionless electrons, nearly totally confined by the electric potential, suggests a nearly isothermal behavior or a mild cooling in a large region of the plasma plume. This approximation is supported by various experimental observations of the far plume, with values in the range $\gamma = 1$–1.3 showing good overall agreement [9–11, 13, 14, 25, 26].

Using this form for the electron pressure in equation (5) gives the following dependence for the plasma potential ϕ:

$$\frac{e\phi}{T_{e0}} = \begin{cases} \ln(n/n_0) & \text{for } \gamma = 1, \\ [(n/n_0)^{\gamma-1} - 1]\gamma/(\gamma-1) & \text{for } \gamma \neq 1, \end{cases} \tag{8}$$

with subscript 0 denoting values at the origin and $\phi_0 \equiv 0$. Likewise, the plasma momentum equation (equation (4) plus equation (5)) becomes

$$m_i(\boldsymbol{u}_i \cdot \nabla)\boldsymbol{u}_i = -\gamma T_e \nabla \ln n. \tag{9}$$

Before proceeding, three comments are needed. First, observe that equations (2) and (9) are coupled and give n and $\boldsymbol{u}_i$. Once n is known, equation (8) yields ϕ and equation (3) gives $\boldsymbol{u}_e$. Note nevertheless that, since the plume needs to be globally current-free, the small electron drift (compared to the thermal motion of the nearly confined electron cloud) satisfies $\boldsymbol{u}_e \simeq \boldsymbol{u}_i$ as a first approximation. This is, in principle, a valid approximation for an unmagnetized plume. A notable exception is the case for thrusters with a magnetic nozzle [27, 28], such as the helicon plasma thruster [29, 30]. In such magnetized plasma expansions, both the local electric currents and the applied magnetic field are dominant features of the expansion [31] and the assumption that $\boldsymbol{u}_e \simeq \boldsymbol{u}_i$ fails. Second, note that the system formed by equations (2) and (9) is analogous to the fluid equations of neutral, non-viscid gas expanding into vacuum. The role of the pressure gradient of the neutral gas case is here taken by the ambipolar electric field, which transmits this force from the electrons to the ions. Thus, the methods to be presented are equally applicable to the case of a hypersonic neutral gas expanding into vacuum, when equivalent conditions are satisfied. Third, observe that a plasma plume model with non-negligible ion temperature that obeys the same thermodynamic assumptions as the electrons and shares the same parameter γ can be immediately reduced to the model presented above by redefining the effective temperature and potential as follows: $T_i + T_e \to T_e$ and $e\,\nabla\phi + \gamma\, T_i\, \nabla \ln(n/n_0) \to e\,\nabla\phi$.

It is convenient to normalize the problem with the values at $z = r = 0$ and a characteristic length such as the initial radius R_0 of the plasma tube $R = R(z)$ carrying 95% of the ion current, i.e.

$$\tilde{z} = z/R_0; \qquad \tilde{r} = r/R_0; \qquad \tilde{R} = R/R_0 \qquad \tilde{n} = n/n_0;$$
$$\tilde{u}_{zi} = u_{zi}/u_{i0}; \qquad \tilde{u}_{ri} = u_{ri}/u_{i0}; \qquad \tilde{T}_e = T_e/T_{e0}; \qquad \tilde{\phi} = e\phi/T_{e0}.$$

In these non-dimensional tilded variables, equation (2) and (9) can be written in cylindrical coordinates as

$$\tilde{u}_{zi}\frac{\partial \ln \tilde{n}}{\partial \tilde{z}} + \tilde{u}_{ri}\frac{\partial \ln \tilde{n}}{\partial \tilde{r}} + \frac{\partial \tilde{u}_{zi}}{\partial \tilde{z}} + \frac{1}{\tilde{r}}\frac{\partial(\tilde{r}\tilde{u}_{ri})}{\partial \tilde{r}} = 0, \tag{10}$$

$$\tilde{u}_{zi}\frac{\partial \tilde{u}_{zi}}{\partial \tilde{z}} + \tilde{u}_{ri}\frac{\partial \tilde{u}_{zi}}{\partial \tilde{r}} = -\frac{\tilde{n}^{\gamma-1}}{M_0^2}\frac{\partial \ln \tilde{n}}{\partial \tilde{z}}, \tag{11}$$

$$\tilde{u}_{zi}\frac{\partial \tilde{u}_{ri}}{\partial \tilde{z}} + \tilde{u}_{ri}\frac{\partial \tilde{u}_{ri}}{\partial \tilde{r}} = -\frac{\tilde{n}^{\gamma-1}}{M_0^2}\frac{\partial \ln \tilde{n}}{\partial \tilde{r}}, \tag{12}$$

where the dependence on the main non-dimensional parameter, the initial ion kinetic energy to electron thermal energy ratio, i.e. the square of the initial ion Mach number:

$$M_0^2 = m_i u_{i0}^2/(\gamma T_{e0}),$$

becomes explicit, with $c_{s0} = \sqrt{\gamma T_{e0}/m_i}$ the ion sonic velocity. Note that $M_0 \simeq 10$–$40 \gg 1$ in the highly hypersonic plume of a plasma thruster.

The resulting hyperbolic ion problem, given by equations (10)–(12), is then closed with the initial profile for both the plasma density n and the ion velocity $\boldsymbol{u}_i$ at the $\tilde{z} = 0$ plane. Introducing a nomenclature that will become useful later, we will refer to these initial conditions as follows:

$$\begin{aligned} &\tilde{n}(0,\tilde{r}) = \nu(\eta); \quad \tilde{u}_{zi}(0,\tilde{r}) = \upsilon(\eta); \\ &\tilde{u}_{ri}(0,\tilde{r})/\tilde{u}_{zi}(0,\tilde{r}) = \delta(\eta), \end{aligned} \tag{13}$$

where the coordinate η represents the normalized radius $\tilde{r}$ at the *initial* plane. The typical shape of these profiles has been plotted in figure 1. Also, we will call α_0 the initial divergence angle of the 95% ion current streamtube, i.e. $\tan(\alpha_0) = \delta$ (1).

The model can be integrated with different approaches. In particular, the method of characteristics (MoC) can be used to integrate numerically equations (10)–(12). In the present work, due to its great accuracy [32], the MoC is used mainly to provide a benchmark solution against which we can compare the results from the semi-analytical integration methods derived in subsequent sections. The MoC technique

is briefly described as follows. In the meridional plane, ion equations present three families of characteristic lines: two Mach lines and the ion streamlines. The slopes of these lines are determined from the plasma properties. After discretizing the initial plasma front into a number of nodes, the characteristic lines are propagated forward and intersected in order to calculate a new plasma front using a predictor–corrector integration scheme, following an approach similar to that in the DIMAGNO code for the plasma expansion in a magnetic nozzle described in [27]. Further detail on the MoC can be found in, for example, [32] or [27].

The MoC integrates supersonic plumes with any given initial profile. However, it involves the full numerical solution of the model and therefore lacks the analytical insight offered by the other two solution methods presented in the following sections. Furthermore, the MoC becomes inadequate in the limit $M_0 \to \infty$, as the three characteristic line families collapse into one (the ion streamlines). This limitation does not affect the semi-analytic methods, which actually require $M_0 \gg 1$ and therefore they complement the MoC in the hypersonic limit.

3. The asymptotic expansion method (AEM)

3.1. The cold plasma limit

One way to reduce the fluid model of section 2 to a tractable analytical expression is to neglect the pressure term, which is equivalent to taking $M_0 \to \infty$ (a fully hypersonic jet). In this cold plasma limit, the plasma momentum equations (11) and (12) (with the right-hand side equal to zero) decouple completely from the continuity equation (10) as the three characteristic line families collapse into one (the ion streamlines). Observe also that no electric potential builds up in this case. The solutions for the velocity and density in this cold plasma limit, which we will call $\tilde{\boldsymbol{u}}_{\rm i}^{(0)}$ and $\tilde{n}^{(0)}$ respectively, depend only trivially on the initial plasma profile functions, ν, υ and δ.

It is immediately seen that $\tilde{\boldsymbol{u}}_{\rm i}^{(0)}$ is simply conserved along the streamlines, which are straight characteristic lines projected from the initial plane ($\tilde{z} = 0$), with radius

$$\tilde{r} = \eta + \delta(\eta)\tilde{z}, \tag{14}$$

where η, their radial position at the initial plane, can be used to label them. Thus, propagating the streamlines to determine the $\eta = \eta(\tilde{z}, \tilde{r})$ map (implicitly given by the equation above) yields $\tilde{u}_{zi}^{(0)}(\tilde{z},\ \tilde{r})$ and $\tilde{u}_{ri}^{(0)}(\tilde{z},\ \tilde{r})$ from the initial plasma profile.

This map can be understood as the transformation of the reference system $(\tilde{z}, \tilde{r})$ into the new reference system $(\zeta,\ \eta)$, where we simply have $\zeta = \tilde{z}$. Differentiation in equation (14) provides the Jacobian matrix J for this transformation:

$$J(\zeta,\eta) = \begin{bmatrix} \partial\tilde{z}/\partial\zeta & \partial\tilde{r}/\partial\zeta \\ \partial\tilde{z}/\partial\eta & \partial\tilde{r}/\partial\eta \end{bmatrix} = \begin{bmatrix} 1 & \delta \\ 0 & 1+\zeta\delta' \end{bmatrix}. \tag{15}$$

In the new coordinates and using these relations, equation (10) allows straightforward integration of the plasma density:

$$\tilde{n}^{(0)}(\zeta,\eta) = \frac{\nu}{(1+\zeta\delta/\eta)(1+\zeta\delta')}, \tag{16}$$

which reflects the decrease in density as the radius of the streamlines increases ($1 + \zeta\ \delta/\eta$) and as they diverge relative to each other ($1 + \zeta\delta'$).

This cold beam solution, while extremely simple, provides a fast first estimate of the plasma plume in the far region as a cone (i.e. without any divergence angle growth). Clearly, the *local* error in the momentum equations is of the order of $1/M^2$, while the global error (the accumulated integration error, i.e. the difference at each point between the exact solution and the approximation) grows with the distance from the initial plane.

Note that this method requires $\delta,\ \delta' \geqslant 0$ to ensure that a clean solution exists everywhere. Were such a condition not met, streamlines would eventually cross, with density gradients going to infinity locally, an indication that pressure effects cannot be neglected around that point.

3.2. First-order corrections

The method presented above can be regarded as the zeroth-order solution for the hypersonic plume when the variables are expanded in the small parameter $\varepsilon = \gamma T_{\rm e0}/(m_{\rm i}u_{\rm i0}^2) \equiv 1/M_0^2$, the initial thermal–kinetic energy ratio in the beam, i.e.

$$\begin{aligned} \tilde{u}_{z\rm i} &= \tilde{u}_{z\rm i}^{(0)} + \varepsilon\tilde{u}_{z\rm i}^{(1)} + \varepsilon^2\tilde{u}_{z\rm i}^{(2)} + \cdots, \\ \tilde{u}_{r\rm i} &= \tilde{u}_{r\rm i}^{(0)} + \varepsilon\tilde{u}_{r\rm i}^{(1)} + \varepsilon^2\tilde{u}_{r\rm i}^{(2)} + \cdots, \\ \ln\tilde{n} &= \ln\tilde{n}^{(0)} + \varepsilon\ln\tilde{n}^{(1)} + \varepsilon^2\ln\tilde{n}^{(2)} + \cdots, \end{aligned} \tag{17}$$

where all terms of order 1 or larger are zero at the initial plane, but grow gradually downstream. The quality of the cold beam solution can be improved substantially by including one or more of these corrections, which allow reducing the local error to $\mathrm{O}(M_0^{-4})$ (for the first order), $\mathrm{O}(M_0^{-6})$ (for the second order), etc. Luckily, the momentum and continuity equations remain decoupled to all orders and can be readily integrated *along the zeroth-order streamlines*, requiring one only to calculate gradients of magnitudes that are already known.

Introducing these expansions into the problem, the first-order correction for the velocity is given by the two plasma momentum equations at order ε, which are solved simultaneously by numerical integration in a single variable (ζ):

$$\upsilon\frac{\partial\tilde{u}_{z\rm i}^{(1)}}{\partial\zeta} + \frac{\upsilon'}{1+\zeta\delta'}(\tilde{u}_{r\rm i}^{(1)} - \tilde{u}_{z\rm i}^{(1)}\delta) = -(\tilde{n}^{(0)})^{\gamma-1}\frac{\partial\ln\tilde{n}^{(0)}}{\partial\tilde{z}}, \tag{18}$$

$$\upsilon\frac{\partial\tilde{u}_{r\rm i}^{(1)}}{\partial\zeta} + \frac{(\upsilon\delta)'}{1+\zeta\delta'}(\tilde{u}_{r\rm i}^{(1)} - \tilde{u}_{z\rm i}^{(1)}\delta) = -(\tilde{n}^{(0)})^{\gamma-1}\frac{\partial\ln\tilde{n}^{(0)}}{\partial\tilde{r}}, \tag{19}$$

where the right-hand sides of the equations are fully known, with the derivative terms left in terms of $\tilde{z}$ and $\tilde{r}$ for compactness.

Once $\tilde{\boldsymbol{u}}_{\rm i}^{(1)}$ is known, the first-order correction to the density is then similarly given by equation (10):

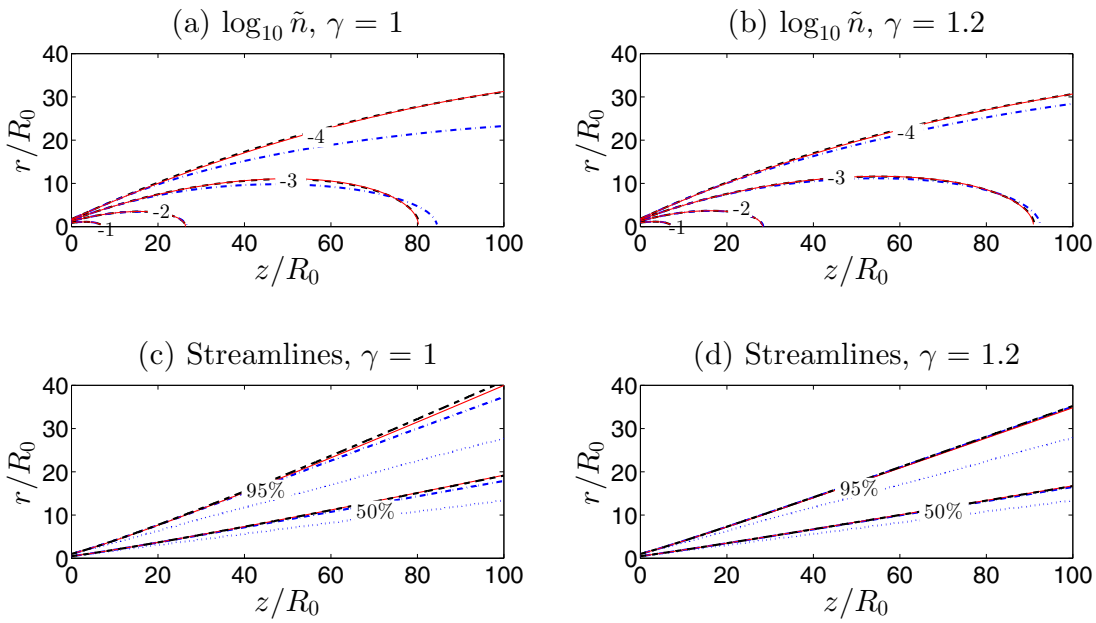

Figure 2. Plasma density contour levels (plots (*a*), (*b*)) and plasma streamtubes containing 50% and 95% of the ion current (plots (*c*), (*d*)) for two plasma plumes with $M_0 = 20$. The second-order AEM is shown in blue dash–dot lines; the SSM is shown in red solid lines; the MoC solution is given in black dashed lines. The dotted blue lines in (*c*) and (*d*) correspond to the cold plasma (conic) approximation, i.e. the zeroth-order AEM. The initial profiles used in this example are the same as those in figure 4(*a*) of [21] but with $\alpha_0 = 15°$.

$$\upsilon\frac{\partial \ln\tilde{n}^{(1)}}{\partial\zeta} = -\tilde{u}_{zi}^{(1)}\frac{\partial \ln\tilde{n}^{(0)}}{\partial\tilde{z}} - \tilde{u}_{ri}^{(1)}\frac{\partial \ln\tilde{n}^{(0)}}{\partial\tilde{r}} - \frac{\partial\tilde{u}_{zi}^{(1)}}{\partial\tilde{z}} - \frac{1}{\tilde{r}}\frac{\partial(\tilde{r}\tilde{u}_{ri}^{(1)})}{\partial\tilde{r}}. \quad (20)$$

It is emphasized that in the expressions above, integrating along ζ means integrating along the *known*, straight, zeroth-order streamlines ($\eta = \text{const}$). The same procedure can be applied to easily obtain higher-order corrections and the general expressions are given in appendix A. Note that the nonlinearity introduced by the ion inertia term and the $\tilde{n}^{\gamma-1}$ term for non-isothermal plumes means that all previous orders contribute to higher-order velocity corrections.

Figure 2 shows the second-order solution of the AEM for a representative initial profile with $\alpha_0 = 15°$, $M_0 = 20$ and two values of γ. Comparison of this solution to the MoC solution shows that a small error develops and grows downstream. Additional simulations show that the error is in all cases larger when M_0 and γ are lower, as expected, due to the larger contribution of pressure effects in a wider region of the plume.

3.3. Region of convergence

For the AEM solution to be valid, the series expansion of equation (17) must converge in the region of interest. Without making any strict statement on the convergence of the series (which depends on the behavior of the ith perturbations as $i \to \infty$), a practical means for exploring the convergence of the method is to equate (in absolute value) the first-order corrections to the zeroth-order solution. The region bounded by this condition is a useful concept for studying the behavior of the first terms in the truncated series and roughly indicates where the error becomes of order 1. In fact, this analysis helps one to determine where to stop the integration and 'reinitialize' the method before the error becomes too large, taking as a new reference plane a section where the plasma properties have already been calculated. This procedure allows extending the AEM solution arbitrarily far downstream with a marching scheme, as well as improving the accuracy obtained.

While the detailed behavior of this region depends on the initial plasma profile, the general behavior can be summarized as follows: the most critical correction is typically the density one, since it grows faster than the velocity correction. As expected, the convergence region extends axially and radially farther downstream for higher M_0 (as the plasma approaches the hypersonic limit) and γ (faster cooling). Thus, the region plotted in figure 3 is shown for $\gamma = 1$, the most restrictive case in terms of convergence. Also, it is found that the three first-order perturbations are generally larger for smaller initial divergence angle, as the divergence growth (and therefore the need for a correction) is greater in that case. In the example of figure 3, $M_0 > 10$ already extends this region far beyond $\tilde{z} = 100$.

4. The self-similar method

Existing measurements and simulations of the far region for GIT and HET beams show the development of a typically smooth, bell-shaped radial plasma profile, which remains essentially invariable along the axial direction, except of course for its radial broadening. This observation suggests modeling the plume expansion as a self-similar phenomenon [22–24]. While the self-similarity assumption is only an approximation, it turns out to be an accurate one for hypersonic plasma plumes.

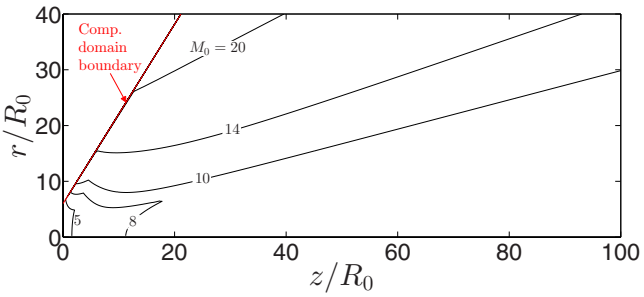

Figure 3. Approximate region of convergence of the AEM for $\gamma = 1$, calculated with the condition that the first-order correction of any one variable be equal to or smaller than the zeroth-order solution. The initial profile is the same as in figure 2.

We first assume that all the streamlines (given again by $\eta = \text{const}$, with η the initial radius of the streamline) expand self-similarly, so their radius is expressed through

$$\tilde{r}(\zeta, \eta) = \eta h(\zeta), \tag{21}$$

where $h(\zeta)$ (with $h\ (0) = 1$) is a self-similarity or dilation function to be determined and ($\zeta = z$, η) can be used again as alternative coordinates for describing the plume. Now, however, the lines $\eta = \text{const}$ are no longer straight as in the AEM. Observe that, once h is determined, we can calculate the ion streamlines directly from it.

We further assume that the initial plasma profiles $\nu(\eta)$ and $\upsilon(\eta)$ are simply propagated in ζ with two scaling functions:

$$\tilde{n} = \nu(\eta)\tilde{n}_c(\zeta), \tag{22}$$

$$\tilde{u}_{zi} = \upsilon(\eta)\tilde{u}_c(\zeta), \tag{23}$$

with $\tilde{n}_c(0) = \tilde{u}_c(0) = 1$. Note that the functions $\tilde{n}_c$ and $\tilde{u}_c$ contain the evolution of the density and the velocity along $\eta = 0$ (the 'centerline', hence the subscript 'c'). Differentiation with respect to time in equation (21) leads to the following basic relation between the velocity components:

$$\tilde{u}_{ri} = \tilde{u}_{zi}\eta h', \tag{24}$$

and its particularization at $\zeta = 0$ reveals a first constraint on the initial plasma profile necessary for finding self-similar solutions, namely, that δ has to be linear in η (i.e. an initially conical velocity profile):

$$\delta' = \text{const}. \tag{25}$$

Using equations (22) and (23) in the continuity equation (equation (10)) leads to

$$h^2\tilde{n}_c\tilde{u}_c = 1, \tag{26}$$

while the radial momentum equation (equation (12)) can be separated in ζ and η as

$$\upsilon^2 = -\frac{\nu^{\gamma-2}\nu'}{\eta C}, \tag{27}$$

$$M_0^2\frac{h\tilde{u}_c(\tilde{u}_c h')'}{\tilde{n}_c^{\gamma-1}} = C, \tag{28}$$

where C is a separation constant. Equation (27) establishes a link between υ and ν, the second constraint on the initial plasma profile required for the SSM to be applicable, from which it is apparent that ν must satisfy $\nu' \leqslant 0$ for all η. Taking $\eta \to 0$ in this equation also gives that $C = -\nu''(0) \neq 0$ for consistency.

So far, we have two equations, equations (26) and (28), to determine the three unknowns h, $\tilde{n}_c$ and $\tilde{u}_c$. The third and last equation should come from the axial momentum equation, equation (11). Unfortunately, trying to apply the same approach to it leaves us with an expression that cannot be separated in ζ, η as before:

$$(\tilde{u}_c^2)' - \tilde{n}_c^{\gamma-2}\tilde{n}_c'\frac{2C\eta^2}{M_0^2}\left(\frac{\nu}{\nu'\eta} - \frac{h'}{h}\frac{\tilde{n}_c}{\tilde{n}_c'}\right) = 0. \tag{29}$$

Moreover, equation (29) renders the system incompatible, since the second term cannot be made independent of η. This proves that no self-similar solutions of this type strictly exist and provides a means for measuring the differential error in the SSM at any point as the residual ϵ_1 of equation (29). Therefore, in order to proceed with the derivation of the approximate SSM, we need to replace equation (29) with an appropriate condition. Incidentally, observe that the AEM becomes self-similar in zeroth order when $\delta' = \text{const}$.

4.1. SSM methods with $\tilde{u}_c = 1$

A convenient replacement for equation (29) in the case of a hypersonic plasma plume is the approximation

$$\tilde{u}_c = \text{const} \equiv 1, \tag{30}$$

which is justified by the fact that relative variations in axial velocity are $O(1/M_0^2)$ and therefore vanishing for $M_0^2 \gg 1$. Thus, the error in the SSM is proportional to M_0^{-2}. The SSM solution in this case follows immediately, with $\tilde{n}_c$ given by equation (26):

$$\tilde{n}_c = 1/h^2, \tag{31}$$

and h being directly integrable from equation (28) (now $h^{2\gamma-1}h'' = C/M_0^2$), using the transformation $h'' = h'\,\mathrm{d}\,h'/\mathrm{d}\,h$:

$$(h')^2 - (h'(0))^2 = \frac{C}{M_0^2} \times \begin{cases} -(h^{2-2\gamma} - 1)/(\gamma - 1) & \text{for } \gamma > 1, \\ 2\ln h & \text{for } \gamma = 1. \end{cases} \tag{32}$$

Equation (32) shows that the slope of h is unbounded in the isothermal case (although its growth is logarithmically slow), whereas for $\gamma \neq 1$ its asymptotic slope is given by

$$(h')^2 \to (h'(0))^2 + 1/(\gamma - 1). \tag{33}$$

The final integration step can be carried out numerically (in the isothermal case the solution is analytical, in terms of $\mathrm{erf}(\zeta)$, the error function). Lastly, the differential error from equation (29) can be written compactly in this case as

$$\epsilon_1 = \frac{C}{M_0^2}\frac{h'}{h^{2\gamma-1}}\left(4\eta\frac{\nu}{\nu'} + 2\eta^2\right), \tag{34}$$

showing that ϵ_1 is only zero for initial plasma profiles with $\nu \propto \eta^{-2}$, which gives a singular condition that cannot be extended down to $\eta = 0$.

Interestingly, it turns out that on fully retaining pressure effects in the $\tilde{r}$ direction and neglecting them in the $\tilde{z}$ direction, the SSM approximation is very accurate even if it is only $O(1/M_0^2)$, as the role of pressure forces on the radial direction is far more important than in the axial direction in a low-divergence plasma plume. In figure 2 the streamlines and density contours for the SSM are plotted and compared against the MoC solution as an illustrative example. As can be seen, except for low values of $\tilde{z}$ and high values of $\tilde{r}$ (for which the AEM yields a better result), the SSM has a solution that is as accurate as or more accurate than the second-order AEM one, in spite of the $O(M_0^{-2})$ error in the $\tilde{z}$ equation.

The only degrees of freedom of the solution, besides the parameters M_0 and γ, are the value of $h'(0)$ (which dictates the initial divergence angle of the plasma plume) and the initial profile, for which only ν or υ can be freely fixed. Parks and Katz [22], Korsun and Tverdokhlebova [24] and Ashkenazy and Fruchtman [23], following different approaches, reached independently three formulations of SSMs and initial profiles, which can be regarded as particularizations of the general SSM framework derived here. These SSMs have been successfully employed to propagate a known plume profile into the far region, as was done e.g. in [26]. In [22], a uniform axial velocity profile is chosen, leading to a Gaussian density profile:

$$\gamma = 1; \quad \nu = \exp(-C\eta^2/2); \quad \upsilon = 1. \tag{35}$$

The local differential error of this SSM cancels out for the streamline $\eta = \sqrt{2/C}$.

In [24] the choice is the following:

$$\nu = \left(1 + C\frac{\eta^2}{2}\right)^{-1}; \quad \upsilon = \left(1 + C\frac{\eta^2}{2}\right)^{-\gamma/2}, \tag{36}$$

which incidentally makes the differential momentum error independent of η.

Lastly, in [23] υ is defined for the isothermal case $\gamma = 1$:

$$\gamma = 1; \quad \nu = (1 + k\eta^2)^{-C/(2k)}; \quad \upsilon = (1 + k\eta^2)^{-1/2}, \tag{37}$$

where k is an arbitrary constant and $(h'(0))^2 = k$ to enforce an initially conical expansion. Observe that on choosing $k = C/2$, this profile coincides with the isothermal model of Korsun *et al* and that for $k \to 0$, it tends to the profile of Parks *et al*. Like in the method of [22], the differential error cancels out for a single streamline. These initial profiles are compared graphically in figure 4(*b*) of [21].

It is important to note that the profile choice in the SSM is not restricted to these three cases or to the condition $\tilde{u}_c = \text{const}$ and that therefore there is a certain freedom (within the aforementioned constraints) to better match the experimental data (see e.g. [26], where the plasma profile is defined from an experimental vector of data) or obtain greater accuracy in the regions of interest. As a last example, we generalize the case $\upsilon = 1$ to non-isothermal plumes:

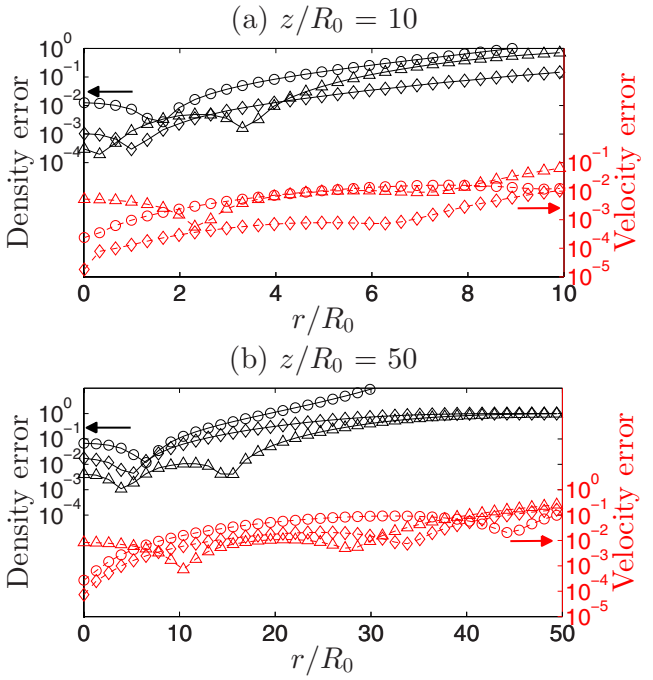

Figure 4. Relative density error (upper, black lines; left vertical axis) and relative velocity magnitude error (lower, red dashed lines; right vertical axis) with respect to the MoC numerical solution, for the AEM (first order: circles; second order: diamonds) and the SSM (triangles) at $\tilde{z} = 10$ (*a*) and 50 (*b*) for the same plasma plumes as in figure 2, with $\gamma = 1.2$.

$$\gamma \neq 1; \quad \nu = \left[1 - (\gamma - 1)C\frac{\eta^2}{2}\right]^{1/(\gamma-1)}; \quad \upsilon = 1. \tag{38}$$

Finally, it is worth discussing also SSMs where $\tilde{u}_c \neq 1$. An interesting alternative to the cases described in this section is the one given by

$$\frac{1}{2}(\tilde{u}_c^2)' = -\frac{\tilde{n}_c^{\gamma-2}}{M_0^2}\tilde{n}_c', \tag{39}$$

which is the ion energy equation (see equation (29)) particularized to the axis of the plume, $\eta = 0$. This choice has the advantage that the local error of the SSM when ignoring the axial momentum equation is zero at the axis, which is of particular importance for applications where the main concern is studying the core of the plume. Since condition equation (27) is not affected by $\tilde{u}_c$, the same profiles as discussed before can be used. As a drawback, in this case $\tilde{u}_c$, h and $\tilde{n}_c$ are coupled through equations (26), (28) and (39), which complicates the solution procedure.

4.2. Discussion of the error and comparison of the methods

The MoC solution can be regarded as exact (except for the numerical truncation error), since it does not introduce any further simplification with respect to the model. However, the MoC necessitates full numerical integration, whereas the semi-analytical AEM and SSM require only minimal numerical work and are therefore markedly faster.

As can be observed in figure 2, both the AEM (at first and second order) and the SSM follow closely the numerical solution of the MoC, with deviations only becoming visible far downstream. The AEM provides a better approximation than the SSM for short distances, especially for the higher-order AEM solutions, while the SSM is in general better suited farther downstream. In return, the AEM can be taken to arbitrary accuracy by adding higher-order correction terms. The region in which the AEM outperforms the SSM becomes larger for higher M_0 and γ. Note that the AEM solutions shown here do not restart the integration on intermediate planes (the downmarching scheme), which would further improve their accuracy.

Figure 4 presents the relative error for each method at $\tilde{z} = 10$ and 50. The largest relative error is typically that in the plasma density. Understandably, since the methods rely on $M_0 \gg 1$, the error depends on M_0 and vanishes for $M_0 \to \infty$ as we approach the cold beam limit. AEM errors are lower than SSM errors at relatively low distances from the initial plane (e.g. $\tilde{z} = 10$). This trend is inverted further downstream (e.g. at $\tilde{z} = 50$). The error also depends on γ, with a purely isothermal plasma (i.e. one that maintains a higher electron pressure downstream) yielding the largest error in both methods, as expected. Finally, the error is also affected by the initial profile. Smoother initial profiles lead in general to a smaller error downstream. A larger initial divergence angle α_0 improves the accuracy of the AEM, but slightly decreases that of the SSM (see figure 8 of [21]).

The main differences between the AEM and the SSM are as follows. Firstly, the AEM allows for more general initial plasma profiles, while the SSM sets stronger constraints on the permitted ν, υ and δ (equations (25) and (27)). This indicates that modeling 'exotic' plasma plumes with unconventional profiles (e.g. the plume with high-density wings observed in the HEMPT (high-efficiency multistage plasma thruster) [33] and DCFT (diverging cusped field thruster) [34] concepts) can only be approached with the AEM (or the MoC). Secondly, each semi-analytical method has a different advantage: the SSM yields the $O(M_0^{-2})$ streamlines directly as part of the solution, whereas the correction terms of the AEM are independent of M_0 (facilitating, for example, parametric studies). As a final comment, observe that the two methods are more adequate than the MoC at high Mach numbers, when the latter is geometrically badly conditioned (the characteristic lines become nearly parallel), thereby complementing it in those cases.

5. Discussion of the plume expansion

The model and solution methods presented allow us to explore the fundamental magnitudes of the expansion of a plasma plume. This section discusses the importance of the ambipolar electric field in the plume, its divergence angle and the limitations of the model in the light of other physical effects.

5.1. The ambipolar electric field

As electrons with temperature T_e expand, the plasma generates an ambipolar electric field $-\nabla\phi \propto T_e$ that confines

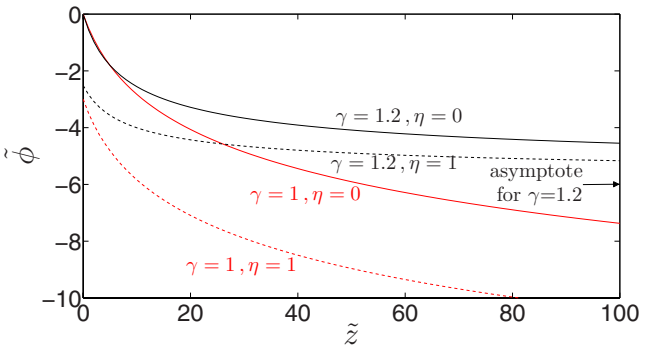

Figure 5. Ambipolar electric potential, $\tilde{\phi}$, along $\eta = 0$ (the axis) and $\eta = 1$ (the 95% ion current tube), for $\gamma = 1$ and 1.2 and the same plasma plumes as in figure 2. The asymptotic value of the potential in the polytropic case is shown on the right. The solution shown is the (exact) MoC solution.

electrons axially and radially. Simultaneously, the presence of this field accelerates ions downstream and raises their divergence angle, becoming a central mechanism of ion transport in the plasma plume. The evolution of $\tilde{\phi} = e\phi/T_{e0}$ along the axis and along $\eta = 1$ is shown in figure 5. A first observation, anticipated already in the derivation of the AEM and the SSM above, is the modest value of $2e\phi/(m_i u_0^2) = 2\tilde{\phi}/M_0^2$ in a highly hypersonic plume ($M_0 \gg 1$). The resulting low axial electric field is responsible for the small axial ion acceleration, which allowed us to assume that $\tilde{u}_c = \text{const}$ as a first approximation in the SSM. In spite of its moderate strength, the ambipolar electric field is the only mechanism in our model responsible for radial ion acceleration and increase of the plasma plume divergence angle.

Secondly, observe that the actual value of $\tilde{\phi}$ is determined by the full kinetic description of the electrons. It is noted that, while the *full* fluid equations are always satisfied in a collisionless plasma (as integral moments of Vlasov's equation), a closure is always needed in a fluid model with a finite number of equations, which affects the thermodynamics of the electrons. In our model, this closure is achieved by assuming isotropic pressure and a polytropic or isothermal expansion, equation (7), leaving the effective cooling rate γ as an additional degree of freedom for matching the experimentally observed behavior of a plume. The relevance of this unknown parameter is evidenced by the appreciable differences between the expansions with $\gamma = 1$ and $\gamma = 1.2$ in figure 2. Observe that another simple closure, not explored here, would be achieved by retaining the electron energy equation and introducing a Fourier law-like heat equation with a constant electron thermal conductivity [25]. These two choices (and any similar approximation) are equally unjustified from a collisionless kinetic viewpoint, neglect the possible anisotropization of the electron population and unavoidably mean a loss of accuracy in the electric field obtained.

The isothermal limit in the model is equivalent to an infinite electron thermal conductivity and to the so-called Boltzmann relation, $\tilde{\phi} = \ln\tilde{n}$ (our equation (8)), widely used in more complex models of plasma plume expansions [4, 18,

35, 36]. In spite of its widespread use, the $\gamma = 1$ limit has the inconvenience of yielding an unrealistic $\tilde{\phi} \to -\infty$ as $\tilde{n} \to 0$, which is approached as the plasma expands downstream. This unbounded decrease of $\tilde{\phi}$ has the following unphysical consequences. Clearly, $\tilde{u}_i \to \infty$, so ions appear to be continuously accelerated (albeit logarithmically slowly). Secondly, sustaining the constant T_e everywhere (in spite of the expansion) and the unbounded ion acceleration require an infinite supply of thermal power for the plasma source, in the form of infinite electron heat fluxes. This impedes the computation of the energy balance in a plasma thruster with an isothermal model. Lastly, $\Delta\tilde{\phi} = -\infty$ means that the spacecraft emitting the plume is floating at an infinite positive potential with respect to the ambient plasma. Hence, Boltzmann's relation (the isothermal limit) is not applicable to an infinite expansion.

This unphysical behavior at infinity is not present if the plasma is allowed to cool at a rate $\gamma > 1$, for which the ambipolar potential exhibits an asymptotic value:

$$\tilde{\phi} \to \tilde{\phi}_\infty = -\frac{\gamma}{\gamma - 1}, \tag{40}$$

as $\tilde{n}, \tilde{T}_e \to 0$, defining an (asymptotic) complete expansion state where the electric field vanishes and $\tilde{u}_i^2 \to \nu^2 (1 + \delta^2) + 2\nu^{\gamma-1}/(M_0^2 (\gamma - 1))$. As stated in section 2, the polytropic model is more consistent with the behavior reported in several laboratory plume experiments. Recent advances in the kinetic modeling of electrons (but in the case of a magnetized expansion [37]) do indeed predict the gradual cooling and anisotropization of electrons downstream, albeit not with a single value of γ for the whole plume domain. Moreover, the inadequacy of $\gamma = 1$ is already apparent in fully kinetic simulations of the first instants of plume formation [38].

Finally, note that the $\eta = 0$ lines in figure 5 depart at about $z \simeq 10R_0$ in this example, a distance at which the isothermal and polytropic models start to yield different results in the central part of the plume.

5.2. The plume divergence angle

The divergence angle is a central figure of merit of a plasma plume. A practical convention for characterizing the divergence angle of the plume and comparing similar thrusters is to consider the angle of the streamtube $\tilde{R}(\tilde{z})$ containing 95% of the plasma flux. Clearly, due to the continued radial expansion, the divergence angle does not remain constant in the far region, but keeps increasing downstream due to the effect of the residual thermal pressure and the ambipolar electric field. To discuss this behavior, we define an *equivalent* far region divergence angle

$$\alpha_F(\tilde{z}_F) = \arctan \frac{\tilde{R}(\tilde{z}_F) - 1}{\tilde{z}_F} \tag{41}$$

as the half-angle of the *cone* that contains 95% of the ion current at a chosen distance from the initial plane (shown in figure 1). Notice that although α_F is a function of $\tilde{z}_F$, (i) α_0 sets a lower boundary to α_F and (ii) this cone is a conservative boundary for that fraction of the ion current within the distance $\tilde{z} \in [0, \tilde{z}_F]$. Calculating the angle α_F allows rapid estimation of the momentum transferred to a surface downstream (following, e.g. the formulation in [39]). Nevertheless, note that α_F does not fully characterize the divergence characteristics of the plume, it being necessary to know the details of the radial plasma profile in order to describe where the ion current (and momentum) is concentrated. This is particularly true for unconventional plumes such as those of the HEMPT [33] or DCFT [34], that can have a hollow central part and most of the current on the plume periphery.

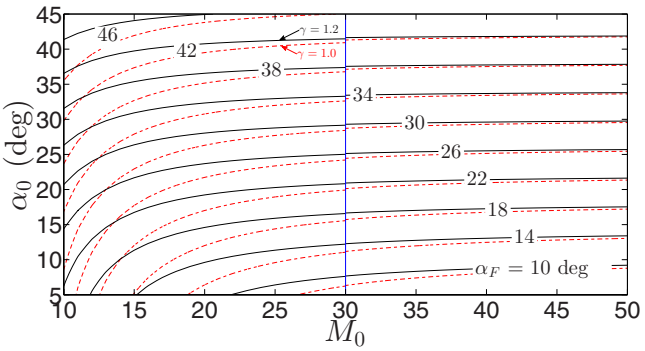

Figure 6. Equivalent far region divergence angle α_F at $\tilde{z} = 50$, as a function of the initial Mach number M_0 and the initial divergence angle α_0. The initial profiles are those of figure 2, adapted to the value of α_0 used. Both the isothermal limit (red dashed lines) and a polytropic plume with $\gamma = 1.2$ (black lines) are shown. The contours have been calculated with the MoC for the lower Mach numbers ($M_0 < 30$) and with the SSM for the larger ones, where the MoC is geometrically less well conditioned (characteristic lines are nearly parallel at high M).

Figure 6 displays the calculated value of α_F at $\tilde{z}_F = 50$ as a function of the two main parameters of the expansion M_0 and α_0 and for two values of γ. Several conclusions can be drawn from this graph.

Firstly, at sufficiently large values of the initial Mach number M_0 (approximately $M_0 > 35$), the effect of the electron pressure becomes negligible and α_F asymptotically approaches α_0. Secondly, at moderate Mach numbers (say, $M_0 < 20$), α_F depends strongly on M_0 and increasing M_0 (whether by imparting a larger acceleration voltage to the ions or by reducing the electron temperature in the plume with a careful neutralizer design) may be more effective in reducing the far region plume divergence than reducing α_0, especially if the latter is already low. Thirdly, α_F is higher for lower γ, for a given M_0 and α_0, due to the electron pressure decaying more slowly closer to the isothermal limit. In fact, while unphysical, the isothermal limit $\gamma = 1$ provides a conservative value of $\alpha_F(\tilde{z}_F)$. Finally, α_F also has a small dependence on the initial density and velocity profile, which, in view of the SSM evolution of the h function (equation (32)), is only second order.

Note that, like for $\tilde{\phi}$, there is no asymptotic value for α_F as $\tilde{z}_F \to \infty$ in the isothermal limit. In contrast, for $\gamma \neq 1$, the equivalent divergence angle has an upper bound and (in

the SSM case) the tangent of the asymptotic α_F is given by equation (33).

5.3. Additional plume physics

While the fluid model has a clear set of assumptions that limit its range of application to collisionless, quasineutral plasma plumes, it is worth exploring, at least qualitatively, the effect and tendencies of other physical phenomena that may be relevant in the expansion.

Near region collisions are an important source for slow charge-exchange ions that may depart at large angles from the axis. Collisions of all types participate in setting up the initial divergence and help homogenize the plume profile; however, they soon become negligible downstream. Consider, as a conservative estimate for a typical propulsive application, a 10 cm thruster that emits a xenon plasma with $n_0 = 10^{18}$ m^{-3}, $T_{e0} = 3$ eV, $u_0 = 30$ km s^{-1}, $\alpha_0 = 15°$ and a mild propellant utilization efficiency of 75% . Assuming that the remaining 25% of the mass flow leaving the thruster is composed of cold neutrals (∼300 K) at their sonic velocity, we have an initial neutral density $n_n \simeq 7 \times 10^{19}$ m^{-3}. At this ion energy, the charge-exchange collision cross-section is roughly [40] 1.6×10^{-19} m^2; hence, the ion mean free path for charge-exchange collisions is already larger than 1 m initially and increases rapidly downstream as n_n and n decrease. Observe that the temperature of neutrals, approximately the temperature of the propellant distributor, plays a minor role in this estimation (to double neutral density and halve the mean free path, the propellant injector has to be at 75 K). Similarly, recombination collisions are infrequent in the plume even in the case of a fast cooling rate and can therefore be neglected for very large distances.

The presence of a sufficiently dense ambient plasma and neutrals can affect the plume expansion in two ways. First, the background plasma will start modifying the solution of the ambipolar potential as soon as its density becomes comparable to the beam density. This could result in (i) an effective cancellation of the expanding electric field, (ii) a limitation to the acceleration of the ions, (iii) the entrainment of background plasma into the plume and/or (iv) the induction of two-stream instabilities in the very far downstream region. Second, background species will slightly enhance collisions due to the additional density. The effects of the background plasma and neutrals are probably largest in vacuum chamber tests due to the limited dynamic pumping capacities, affecting the quality of the peripheral and far region measurements that can be taken in the laboratory. In space operation, however, the main practical effect of the background plasma ($n \sim 10^{11}$ m^{-3} in low Earth orbit) is probably to set a limit to the total $\Delta\phi$ along the plume, as ϕ_∞ must match the background potential and the satellite cannot float very positively due to negative spacecraft charging by the ambient electrons. Hence, this effect may work together with the plasma cooling described above to set the actual ϕ_∞.

Finally, the presence of an ambient magnetic field $\boldsymbol{B}$ such as the geomagnetic field (≃0.5 G at low Earth orbit) can deform the shape of the plume by magnetizing and guiding the trajectories of the light electrons. Macroscopically, the external magnetic field induces electric currents $\boldsymbol{j}$ on the plume. Concurrently, these currents induce a plasma-generated magnetic field that opposes and tends to expel the external one from the core of the plasma (i.e. the currents are diamagnetic). The relative importance of the induced magnetic field compared with the external one is given by the total beta parameter [41], which relates the energy available in the plasma and the energy of the external magnetic field:

$$\beta_{tot} = n(T_e + m_i u_i^2/2)/(B^2/\mu_0). \quad (42)$$

A value $\beta_{tot} \gg 1$ indicates dominant induced field effects and that the external field therefore only perturbs the thinner peripheral plasma. For the same numerical example as above with $n_0 = 10^{18}$ m^{-3}, we need to travel more than 20 m downstream before $\beta_{tot} < 1$, which suggests a strong expulsion of the external magnetic field from the core of the beam up to long distances. The electric currents in the plasma also experience the Lorentz force $\boldsymbol{j} \times \boldsymbol{B}$. This force distorts the plume expansion depending on the direction of the magnetic field with respect to the axis of the plume, possibly affecting its divergence. As suggested in [42], the magnetic field would flatten the plume in the direction perpendicular to both $\boldsymbol{B}$ and the axis of the plume, along which the transport is hindered and stretch it in the plane defined by $\boldsymbol{B}$ and the axis. This behavior of the plume is of particular concern for spacecraft charging and contamination studies, where we are interested in determining precisely the ion flux to a given satellite surface.

Notwithstanding this, a qualitative analysis shows that a uniform external magnetic field $\boldsymbol{B}_0$ can deform, but not deflect, a globally current-free plasma plume. Indeed, assuming that no electrical currents flow into or out of the plasma domain or to infinity, the total magnetic force on the whole plasma domain Ω is zero, since the induced magnetic field forces are purely internal, and for the external field

$$\boldsymbol{F}_{plume} = \int_\Omega \boldsymbol{j} \times \boldsymbol{B}_0 \, d\Omega = \left(\int_\Omega \boldsymbol{j} \, d\Omega \right) \times \boldsymbol{B}_0 = 0, \quad (43)$$

where the integral in parentheses is zero since no current flows into or out of the volume (i.e. for each vector component of the integral, e.g. x, we have $\int j_x \, dy \, dz = 0$ over a yz cross-section of the plume).

6. Conclusions

The behavior of hypersonic plasma plumes has been studied with a two-fluid model, which has been integrated with two semi-analytic solution methods (AEM and SSM) and the MoC. The AEM and SSM methods both yield approximate solutions and each has its own advantages. The AEM method enables one to reach arbitrary accuracy in a limited region, can be used to set up a marching integration scheme and provides more flexibility in the choice of initial density and velocity profiles, allowing the study of complex plumes. An additional

advantage of the AEM is that the perturbation terms themselves are independent of M_0 and can be reused to explore the effect of different Mach numbers on the expansion without recalculating the solution each time (useful e.g. for parametric studies). The SSM, in contrast, is algebraically simpler and provides the ion streamlines directly as part of the solution (the h function) for a limited range of initial plasma profiles and a relatively easy calculation with an accurate solution in a wider region.

The relative errors of the AEM and the SSM in density and velocity, as compared with the MoC exact solution, are small in all of the cases studied (10^{-2}–10^{-3} at 50 thruster radii downstream at the axis). Both methods are particularly accurate near the hypersonic limit where the MoC is geometrically badly conditioned (Mach lines become nearly parallel at high M), thereby complementing the MoC (more appropriate for problems with $M_0 \gtrsim 1$).

The electron thermodynamics, through the effective cooling rate γ, have been shown to condition the electron expansion, the evolution of the ambipolar plasma potential and the divergence angle growth rate. The isothermal limit, $\gamma = 1$, which yields the well-known Boltzmann relation, leads to unphysical results at infinity, indicating that there must exist a collisionless cooling mechanism in the plume and revealing the inadequacy of Boltzmann's relation for infinite expansions.

The equivalent divergence angle α_F at a given downstream section depends fundamentally on M_0^2 (and, conversely, on the ratio of the beam accelerating voltage to the electron temperature in the plume) and α_0. An important observation is that in order to decrease α_F it may be more advantageous to increase the ion Mach number M_0 (i.e. increase the voltage or limit the electron temperature in the plume) than to decrease the initial divergence angle α_0, which can be more challenging in certain thruster designs, especially at lower Mach numbers and already low divergence angles ($M_0 < 20$ and $\alpha_0 < 20°$). As regards α_F, $\gamma = 1$ yields the upper bound for the plume divergence angle.

Lastly, several physical aspects of plasma plumes not included in the fluid model have been briefly discussed and will be subjects of future work. Collisions and recombination have been shown to be negligible in the far plume, while electron kinetic effects can play a major role in the expansion and warrant detailed modeling. A dense ambient plasma or a neutral species could alter the expansion of the plume. Finally, a background magnetic field can distort the expansion of the plasma profile, but—at least under certain assumptions—not its propagation direction.

Acknowledgments

The research leading to these results received funding from the European Union Seventh Framework Program (FP7/2007-2013) under grant agreement number 607457. Additional support was provided by the Spanish R&D National Plan (grant number ESP2013-41052-P). Preliminary versions of this work were presented at two conferences [20, 21].

Appendix A

The ith-order correction to the velocity in the AEM solution is given by the following equations, which are integrated in the same fashion as the first-order correction:

$$\upsilon\frac{\partial \tilde{u}_{zi}^{(i)}}{\partial\zeta} + \frac{\upsilon'}{1+\delta'\zeta}(\tilde{u}_{ri}^{(i)} - \tilde{u}_{zi}^{(i)}\delta) = -\sum_{j=1}^{i-1}\left(\tilde{u}_{zi}^{(j)}\frac{\partial \tilde{u}_{zi}^{(i-j)}}{\partial\tilde{z}} + \tilde{u}_{ri}^{(j)}\frac{\partial \tilde{u}_{zi}^{(i-j)}}{\partial\tilde{r}}\right) - \sum_{j=1}^{i}\mathcal{T}_\varepsilon(\tilde{n}^{\gamma-1}, \varepsilon^{j-1})\frac{\partial \ln\tilde{n}^{(i-j)}}{\partial\tilde{z}}, \tag{A.1}$$

$$\upsilon\frac{\partial \tilde{u}_{ri}^{(i)}}{\partial\zeta} + \frac{(\upsilon\delta)'}{1+\delta'\zeta}(\tilde{u}_{ri}^{(i)} - \tilde{u}_{zi}^{(i)}\delta) = -\sum_{j=1}^{i-1}\left(\tilde{u}_{zi}^{(j)}\frac{\partial \tilde{u}_{ri}^{(i-j)}}{\partial\tilde{z}} + \tilde{u}_{ri}^{(j)}\frac{\partial \tilde{u}_{ri}^{(i-j)}}{\partial\tilde{r}}\right) - \sum_{j=1}^{i}T_\varepsilon(\tilde{n}^{\gamma-1}, \varepsilon^{j-1})\frac{\partial \ln\tilde{n}^{(i-j)}}{\partial\tilde{r}}, \tag{A.2}$$

where $\mathcal{T}_\varepsilon(\tilde{n}^{\gamma-1}, \varepsilon^{j-1})$ denotes the coefficient of ε^{j-1} of the Taylor series of $\tilde{n}^{\gamma-1}$ in ε, which results from expanding the following expression:

$$\tilde{n}^{\gamma-1} = (\tilde{n}^{(0)})^{\gamma-1}\cdot\left(1 + (\gamma-1)\varepsilon\ln\tilde{n}^{(1)} + \tfrac{(\gamma-1)^2}{2}\varepsilon^2\ln^2\tilde{n}^{(1)} + \cdots\right)\cdot\left(1 + (\gamma-1)\varepsilon^2\ln\tilde{n}^{(2)} + \tfrac{(\gamma-1)^2}{2}\varepsilon^4\ln^2\tilde{n}^{(2)} + \cdots\right)\cdot(\cdots). \tag{A.3}$$

Similarly, the ith correction to the density is then given by

$$\upsilon\frac{\partial \ln\tilde{n}^{(i)}}{\partial\zeta} = -\sum_{j=1}^{i}\left(\tilde{u}_{zi}^{(j)}\frac{\partial \ln\tilde{n}^{(i-j)}}{\partial\tilde{z}} + \tilde{u}_{ri}^{(j)}\frac{\partial \ln\tilde{n}^{(i-j)}}{\partial\tilde{r}}\right) - \frac{\partial \tilde{u}_{zi}^{(i)}}{\partial\tilde{z}} - \frac{1}{\tilde{r}}\frac{\partial(\tilde{r}\tilde{u}_{ri}^{(i)})}{\partial\tilde{r}}. \tag{A.4}$$

References

[1] Goebel D and Katz I 2008 *Fundamentals of Electric Propulsion: Ion and Hall Thrusters* (New York: Wiley)
[2] Ahedo E 2011 *Plasma Phys. Control. Fusion* **53** 124037
[3] Garrett H 1981 *Rev. Geophys.* **19** 577–616
[4] Boyd I 2001 *J. Spacecr. Rockets* **38** 380
[5] Bombardelli C and Peláez J 2011 *J. Guid. Control Dyn.* **34** 916–20
[6] Merino M, Ahedo E, Bombardelli C, Urrutxua H and Peláez J 2013 Ion beam shepherd satellite for space debris removal *Progress in Propulsion Physics (EUCASS Advances in Aerospace Sciences* vol 4*)* ed L T DeLuca *et al* (Moscow: Torus) chapter 8, pp 789–802
[7] Bombardelli C, Urrutxua H, Merino M, Ahedo E and Peláez J 2013 *Acta Astronaut.* **90** 98–102
[8] Aston G, Kaufman H and Wilbur P 1978 *AIAA J.* **16** 516–24
[9] Foster J, Soulas G and Patterson M 2000 Plume and discharge plasma measurements of an NSTAR-type ion thruster *36th*

AIAA/ASME/SAE/ASEE Joint Propulsion Conf. and Exhibit (Washington, DC: AIAA) AIAA 2000–3812
[10] Beal B, Gallimore A and Hargus W 2005 *Phys. Plasmas* **12** 123503
[11] Brieda L, Garrett D R and Randy R 2007 Experimental and numerical examination of the BHT-200 Hall thruster plume *43rd AIAA/ASME/SAE/ASEE Joint Propulsion Conf. and Exhibit* (Washington, DC: AIAA) AIAA 2007–5305
[12] Martinez-Sanchez M and Pollard J E 1998 *J. Propulsion Power* **14** 688–99
[13] Myers R and Manzella D 1993 Stationary plasma thruster plume characteristics *23rd Int. Electric Propulsion Conf.* (Fairview Park, OH: Electric Rocket Propulsion Society) IEPC 93–096
[14] Beal B, Gallimore A, Hargus W A and Blandino J H 2004 *J. Propulsion Power* **20** 985–91
[15] Absalamov S *et al* 1992 Measurement of plasma parameters in the stationary plasma thruster (SPT-100) plume and its effect on spacecraft components *28th AIAA/ASME/SAE/ASEE Joint Propulsion Conf.* (Washington, DC: AIAA) AIAA 92–3156
[16] King L and Gallimore A 2000 *J. Propulsion Power* **16** 916–22
[17] Dannenmayer K, Kudrna P, Tichy M and Mazouffre S 2011 *Plasma Sources Sci. Technol.* **20** 065012
[18] Oh D, Hasting D, Marrese C, Haas J and Gallimore A 1999 *J. Propulsion Power* **15** 345–57
[19] Celik M, Santi M, Cheng S, Martínez -Sánchez M and Peraire J 2003 Hybrid-PIC simulation of a Hall thruster plume on an unstructured grid with DSMC collisions *28th Int. Electric Propulsion Conf.* (Fairview Park, OH: Electric Rocket Propulsion Society) IEPC 03–134
[20] Merino M, Ahedo E, Bombardelli C, Urrutxua H and Peláez J 2011 Hypersonic plasma plume expansion in space *32nd Int. Electric Propulsion Conf.* (Fairview Park, OH: Electric Rocket Propulsion Society) IEPC 2011–086
[21] Cichocki F, Merino M and Ahedo E 2014 Modeling and simulation of EP plasma plume expansion into vacuum *50th AIAA/ASME/SAE/ASEE Joint Propulsion Conf. and Exhibit* (Washington, DC: AIAA) AIAA 2014–3828
[22] Parks D and Katz I 1979 A preliminary model of ion beam neutralization *14th Int. Electric Propulsion Conf.* (Fairview Park, OH: Electric Rocket Propulsion Society) IEPC 79–2049
[23] Korsun A and Tverdokhlebova E 1997 The characteristics of the EP exhaust plume in space *33rd AIAA/ASME/SAE/ASEE Joint Propulsion Conf. and Exhibit* (Washington, DC: AIAA)
[24] Ashkenazy J and Fruchtman A 2001 Plasma plume far field analysis *27th Int. Electric Propulsion Conf.* (Fairview Park, OH: Electric Rocket Propulsion Society) IEPC 01–260
[25] Cohen-Zur A, Fruchtman A and Gany A 2008 *IEEE Trans. Plasma Sci.* **36** 2069–81
[26] Dannenmayer K, Mazouffre S, Ahedo E and Merino M 2012 Hall effect thruster plasma plume characterization with probe measurements and self-similar fluid models *48th AIAA/ASME/SAE/ASEE Joint Propulsion Conf. and Exhibit* (Washington, DC: AIAA) AIAA 2012–4117
[27] Ahedo E and Merino M 2010 *Phys. Plasmas* **17** 073501
[28] Ahedo E and Merino M 2011 *Phys. Plasmas* **18** 053504
[29] Charles C, Boswell R and Lieberman M 2006 *Appl. Phys. Lett.* **89** 261503
[30] Ahedo E and Navarro J 2013 *Phys. Plasmas* **20** 043512
[31] Merino M and Ahedo E 2014 *Plasma Sources Sci. Technol.* **23** 032001
[32] Zucrow M and Hoffman J 1976 *Gas Dynamics* (New York: Wiley)
[33] Koch K and Schirra M 2011 The HEMPT concept: a survey on theoretical considerations and experimental evidences *32nd Int. Electric Propulsion Conf.* (Fairview Park, OH: Electric Rocket Propulsion Society) IEPC 2011–236
[34] Courtney D and Martínez -Sánchez M 2007 Diverging cusped-field Hall thruster *30th Int. Electric Propulsion Conf.* (Fairview Park, OH: Electric Rocket Propulsion Society) IEPC 2007–39
[35] Mikellides I G, Jongeward G A, Gardner B M, Katz I, Mandell M J and Davis V A 2001 A Hall-effect thruster plume and spacecraft interactions modeling package *27th Int. Electric Propulsion Conf.* (Fairview Park, OH: Electric Rocket Propulsion Society) IEPC 01–251
[36] Garrigues L, Bareilles J and Boeuf J P 2002 *J. Appl. Phys.* **91** 9521
[37] Navarro-Cavallé J, Martínez-Sánchez M and Ahedo E 2014 Collisionless electron cooling in a magnetic nozzle *50th AIAA/ASME/SAE/ASEE Joint Propulsion Conf. and Exhibit* (Washington, DC: AIAA) AIAA 2014–4028
[38] Hu Y and Wang J 2014 Fully kinetic simulations of collisionless, mesothermal plasma expansion *13th Spacecraft Charging Technology Conf.*
[39] Bombardelli C, Urrutxua H, Merino M, Ahedo E and Peláez J 2012 Relative dynamics and control of an ion beam shepherd satellite *Spaceflight Mechanics (Advances in the Astronautical Sciences* vol 143*)* ed J V McAdams *et al* (San Diego, CA: Univelt) pp 2145–58
[40] Rapp D and Francis W 1962 *J. Chem. Phys.* **37** 2631–45
[41] Brenning N, Hurtig T and Raadu M 2005 *Phys. Plasmas* **12** 012309
[42] Korsun A, Tverdokhlebova E and Gabdullin F 2004 *Comput. Phys. Commun.* **164** 434–41